

RSC Advances



This is an *Accepted Manuscript*, which has been through the Royal Society of Chemistry peer review process and has been accepted for publication.

Accepted Manuscripts are published online shortly after acceptance, before technical editing, formatting and proof reading. Using this free service, authors can make their results available to the community, in citable form, before we publish the edited article. This *Accepted Manuscript* will be replaced by the edited, formatted and paginated article as soon as this is available.

You can find more information about *Accepted Manuscripts* in the [Information for Authors](#).

Please note that technical editing may introduce minor changes to the text and/or graphics, which may alter content. The journal's standard [Terms & Conditions](#) and the [Ethical guidelines](#) still apply. In no event shall the Royal Society of Chemistry be held responsible for any errors or omissions in this *Accepted Manuscript* or any consequences arising from the use of any information it contains.

Modulating the permeability of the ferritin channels †

C. Bernacchioni,^{a,b} V. Ghini,^{a,b} E. C. Theil,^{c,d} and P. Turano^{*a,b}

Received 00th January 20xx,
Accepted 00th January 20xx

DOI: 10.1039/x0xx00000x

www.rsc.org/

Twentyfour-mer ferritins are present in all kingdoms of life and play an essential role as iron storage proteins. The formation of a caged iron biomineral is driven by enzymatic reaction occurring at ferroxidase centers in the central part of ferroxidase catalytically-active subunits, where Fe²⁺ is the reaction substrate. To this purpose, Fe²⁺ needs to be translocated through the protein cage. Two different types of channels pierce the ferritin nanocage, in correspondence of C3 and C4 symmetry axes. The polarity across the channels controls the directional Fe²⁺ fluxes towards the ferroxidase center. In vertebrate ferritins, the C3 channels have been identified as the entry ion channels coupled with the ferroxidase reaction. Here, we have prepared a series of variants of the ferritin nanocage to study the role of electrostatic residues inside the two types of channels in directioning Fe²⁺ substrates towards the catalytic ferroxidase site and the inner biomineralization cavity. Interestingly, by changing the electrostatic properties of the residues at the inner edge of each channel, we can selectively activate/deactivate Fe²⁺ routes, modulating the rate of iron oxidation at the ferroxidase sites.

Introduction

Ferritins, the ubiquitous intracellular iron-storage proteins, are nanocages that self-assemble from 24 subunits into a hollow structure with an 8 nm-diameter internal cavity¹ (Fig. 1). The resulting architecture has 432 (O, octahedral) point symmetry. The 3-fold (C3) and 4-fold (C4) symmetry axes intersect the protein shell in correspondence to eight and six channels, respectively, connecting the protein exterior to the inner cavity²⁻⁴. These channels are about 2 nm long and their chemical features are determined by the properties of residues at the subunit polymerization interfaces at the C3 and C4 symmetry axes.

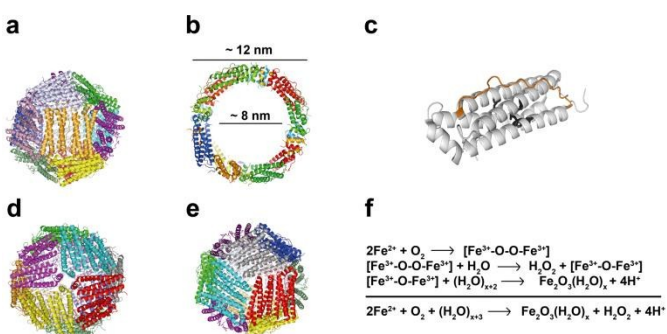


Fig. 1. Nanocage structure of *Rana catesbeiana* H' ferritin. (a) External view of the nanocage; pairs of subunits interacting along the C2 symmetry axes are shown with the same color. (b) Cross section of the nanocage showing the large inner cavity. (c) The ferritin subunit, with the 4-helix bundle helices (H1–H4) and the short helix H5 shown in gray; the iron ligands at the ferroxidase site in black sticks; and the external inter-helical loop in orange. (d) Four symmetry-related subunits generate the C4 pores. (e) Three symmetry-related subunits form the C3 ion channels. Drawn using PyMOL and the PDB file 4DAS. (f) The multistep iron biomineralization reaction in ferritin.

The protein subunits in ferritins from different organisms share a common fold: a 4-helix bundle structure (helices H1–H4) completed by a short C-terminal helix, H5, and a long loop connecting H2 and H3 (Fig. 1c). The most extended intersubunit contacts occur along 2-fold symmetry axes between pairs of antiparallel-coupled subunits and involve helices H1, H2 and the loop^{1,5}. Adjacent pairs of subunits in assembled nanocages are essentially orthogonal one to another (Fig. 1a). Six channels with C4 symmetry form at the encounter point between the C-termini of four subunits from different pairs (Fig. 1d): the four symmetry-related H5 helices define the inner wall of the channel (Fig. 1d). C3 channels (Fig. 1e) occur where three subunits from different pairs come into contact through the N-terminal ends of helices H4 and the C-terminal hands of helices H3. Catalytically active subunits contain a ferroxidase (or oxidoreductase) center (Fe1–Fe2)⁶ where oxidation of 2 Fe²⁺ by oxygen occurs when diferrous substrate centers are established (reaction in Fig. 1f)^{7,8}. The ferroxidase site is invariably located in the inner part of the 4-helix bundle, midway from the subunit edges defining the wall of the C3 and C4 channels. In vertebrate ferritins, high sequence conservation between H/H' subunits, which contain ferroxidase enzymatic centers, and L subunits, which lack this type of catalytic sites, ensures conservation of channel

^aCERM, University of Florence, Via Luigi Sacconi 6, 50019 Sesto Fiorentino, Italy.

^bDepartment of Chemistry, University of Florence, Via della Lastruccia 3, 50019 Sesto Fiorentino, Italy.

^cChildren's Hospital Oakland Research Institute, 5700 Martin Luther King, Jr. Way, Oakland, CA, 94609, USA

^dDepartment of Molecular and Structural Biochemistry, North Carolina State University, Raleigh, NC, 27695-7622, USA

† Electronic Supplementary Information (ESI) available: [Alignment of the amino acid sequence of subunits from divergent branches of the ferritin phylogenetic tree] See DOI: 10.1039/x0xx00000x

features, regardless of the H:L ratio in the 24-mer cage (Fig. S1). The H5 helices expose neutral and mainly hydrophobic residues in the inner part of the narrow C4 channels; the eight C3 channels are wider and negatively charged. Consequently, in vertebrate ferritins the ferrous ions enter the cavity through the C3 channels. As observed in high resolution X-ray structures of *Rana catesbeiana* H' ferritin⁹ and human H ferritin¹⁰, the entering species are ferrous hexa-aqua ions, transiently interacting with the carboxylate groups of D127 and E130 at the bottom of the channel. From this site, the ferrous species then proceed toward the ferroxidase sites in the middle of 4-helix bundle subunits^{6,10-15}. In vertebrate ferritins access to the cage through the C3 channels is a forced passage that relies on the presence of the carboxylate groups at the bottom end of the C3 channels. Substitution of these negatively charged residues with neutral ones reduces the iron uptake and therefore the efficiency of the ferroxidase reaction at ferroxidase sites^{6,11-15}. On the contrary, the C4 channels are not viable to ferrous species because narrower and largely hydrophobic; transit of iron species through these channels is not observed in crystal even after long times of free Fe²⁺ diffusion^{9,10}. The maintenance of the gross cage architecture and conservation of the iron ligand residues in the ferroxidase site across ferritins from different species notwithstanding, the interior of the C3 and C4 channels are quite variable: there are substantial differences in the hydrophilicity and electric charge distributions when comparing vertebrate ferritins with those from plants, bacteria or archaea. The properties of the

channels determine the pathway driving the ferrous substrate from the exterior of the cage to the ferroxidase center.

Here, we show that interchanging the electrostatic properties of the two types of channels in vertebrate ferritins leads to an enzymatically active nanocage, able to efficiently form and retain the iron biomineral. The work provides evolutionary insight, suggesting that the non-conservation of the channels' properties across different species might be the result of a divergent evolution that leads to comparably active species rather than a selection of the maximum ferroxidase efficiency.

Results and discussion

Study design. Previous calculations of the electrostatic potential energy have shown that the deep carboxylates in the C3 channels are essential for the attraction of the divalent iron ions¹⁶. These theoretical data support mutational studies performed on frog H' and human H and L ferritins reporting severe reduction in the ferroxidase activity (in H' and H ferritin) and iron incorporation (in L ferritin) when these carboxylates have been replaced by neutral residues^{13-15,17-19}. The aim of the present study was to verify whether, using the H' ferritin scaffold, it is possible to invert the directionality of the ferrous pathways by selectively activating C4 channels as ion entry channels. To this purpose, we have designed multiple protein variants (Fig. 2).

a

ACRONYM	DESCRIPTION	MUTATIONS
WT	negatively charged C3 (C3 ^{ON}) apolar C4 (C4 ^{OFF})	none
C3 ^{OFF} C4 ^{OFF}	apolar C3 (C3 ^{OFF}) apolar C4 (C4 ^{OFF})	D127AE130AS131A
C3 ^{OFF} C4 ^{ON}	apolar C3 (C3 ^{OFF}) negatively charged C4 (C4 ^{ON})	D127AE130AS131A- M161DL165DH169D
C3 ^{ON} C4 ^{ON}	negatively charged C3 (C3 ^{ON}) negatively charged C4 (C4 ^{ON})	M161DL165DH169D

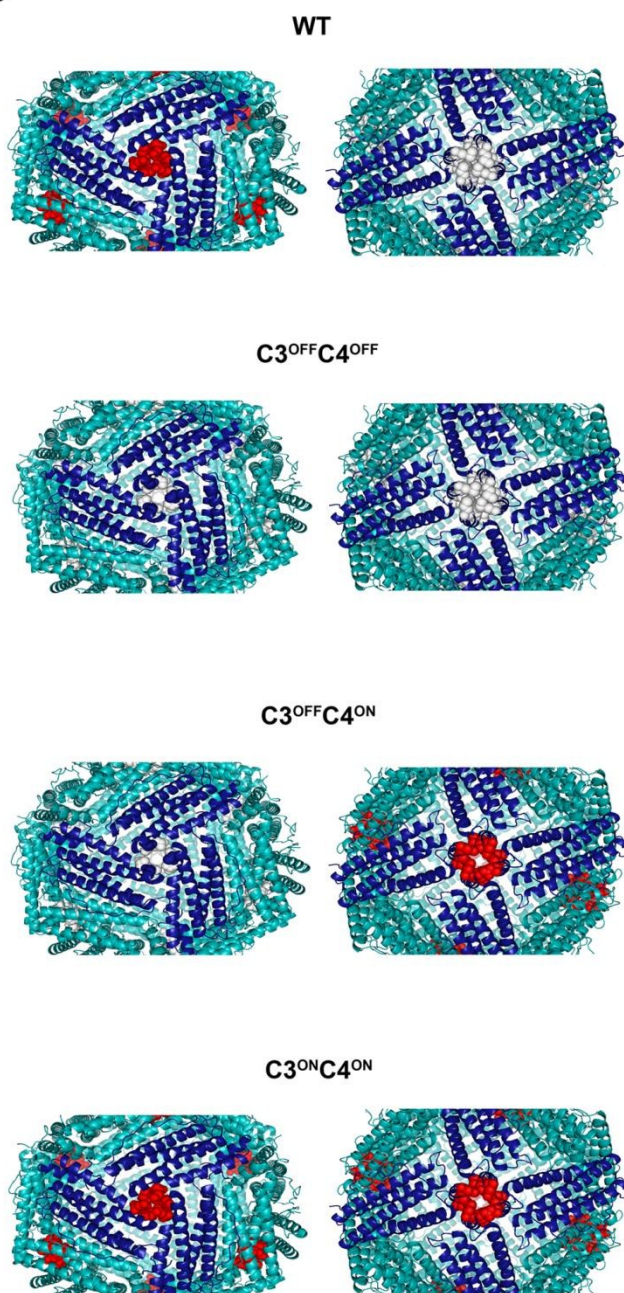
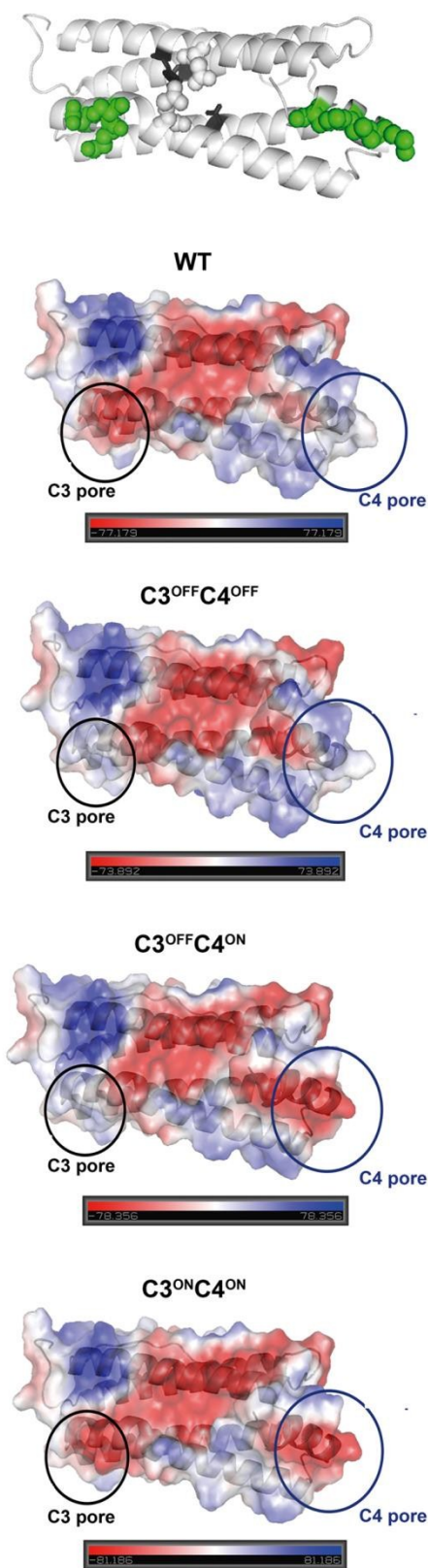
b**c**

Fig. 2. Modulation of Fe²⁺ entry points in ferritin variants. (a) The amino acid substitutions in the different ferritin variants and the resulting electrostatic

properties of the pores. (b) Cartoon representation of the C3 and C4 pores seen from the external surface. Left panel, three symmetry-related subunits form the

C3 ion channel; right panel, four symmetry-related subunits form the C4 ion channel. Mutated residues are shown as white spheres when Ala and red spheres when Asp/Glu/Ser. A widening from about 4.3 Å in WT (C4^{OFF}) to about 7.0 Å in C4^{ON} pores, and from about 5.8 Å in WT (C3^{ON}) to about 9.5 Å in C3^{OFF} pores is observed. (c) View of the inner surface of each subunit. Cartoon representation of the WT subunit highlighting the residues considered for mutations as green spheres, the Glu57/Glu136 pair as grey spheres and the ferroxidase site residues as black sticks (upper panel). Lower panels show the internal surface potential of a single subunit of the different ferritin variants described in panel a. Circles identify the position of the two type of channels. Panels b and c were drawn with PyMOL using the PDB file 4DAS and corresponding model structures of the variant ferritins.

The mutation sites were selected by visual inspection of the cage surface potentials. The new charge distributions were calculated on the energy-minimized modeled structures of the ferritin variants (Fig. 2c).

The biomineralization reaction in ferritin proceeds through a multistep process (Fig. 1f). The formation of transient diferric-peroxo (DFP) intermediates and diferric-oxo/hydroxo (DFO(H)) precursors of the biomineral occurs at the ferroxidase site on the second time scale⁷; the biomineral forms in the inner cage on a much longer time scale. At low Fe²⁺/subunit ratio, the efficiency of the iron transit through the channels is monitored by measuring the kinetics at the ferroxidase site. The effects of the channel mutations on the kinetic of the ferroxidase reaction were evaluated following the formation of DFP intermediates and DFO(H) precursors at the active site by monitoring the absorbance changes at 650 and 350 nm, respectively (Fig. 3 and 4). The structure integrity and the ability to form and retain the biomineral were verified, respectively, by elution profiles in gel filtration chromatography (Fig. S2) and circular dichroism (CD; Fig. 3b) and by transmission electron microscopy (TEM) and magnetic susceptibility measurements (Fig. 5).

Ferroxidase activity. In vertebrate ferritins, the C3 are the ion channels through which Fe²⁺ enters the cage^{6,10-15,17-19}. Replacing with Ala the three residues responsible of the negative surface electrostatic potential at the bottom edge of the C3 channels in the wild type (WT) cage provided a ferroxidase catalytically inactive D127AE130AS131A ferritin (Fig. 3a). This variant is hereafter called C3^{OFF}C4^{OFF} (Fig. 2) to highlight the properties of the two types of channels: i) with these mutations, the C3 channels have lost their permeability to the ferrous aqua ions; ii) the C4 channels in their WT form are not viable for ferrous ions entry, as shown by the lack of any enzymatic activity when switching off the C3 channels while leaving the C4 intact. In this study, the D127AE130AS131A, C3^{OFF}C4^{OFF} variant is the archetypical ferroxidase inactive cage. Consistently, the WT “phenotype” is C3^{ON}C4^{OFF} (Fig. 2). While maintaining the C3^{OFF} (D127AE130AS131A), we have then designed a ferritin variant with altered C4 channel electrostatics. By mirroring the negative charge distribution of the WT structure at the C3 channels on the C4 channels (Fig. 2c), three carboxylates have been introduced at the bottom end of the C4 channels, providing the M161DL165DH169D variant (Fig. 2). In our

working hypothesis, these mutations should create an attractive electrostatic gradient towards cations at the C4 channels, providing a C3^{OFF}C4^{ON} phenotype. Consistently, the ferroxidase activity was fully restored (Fig. 3a), as shown by the comparison of the reaction kinetics with 2 Fe²⁺/subunit between C3^{OFF}C4^{ON} and the WT (C3^{ON}C4^{OFF}).

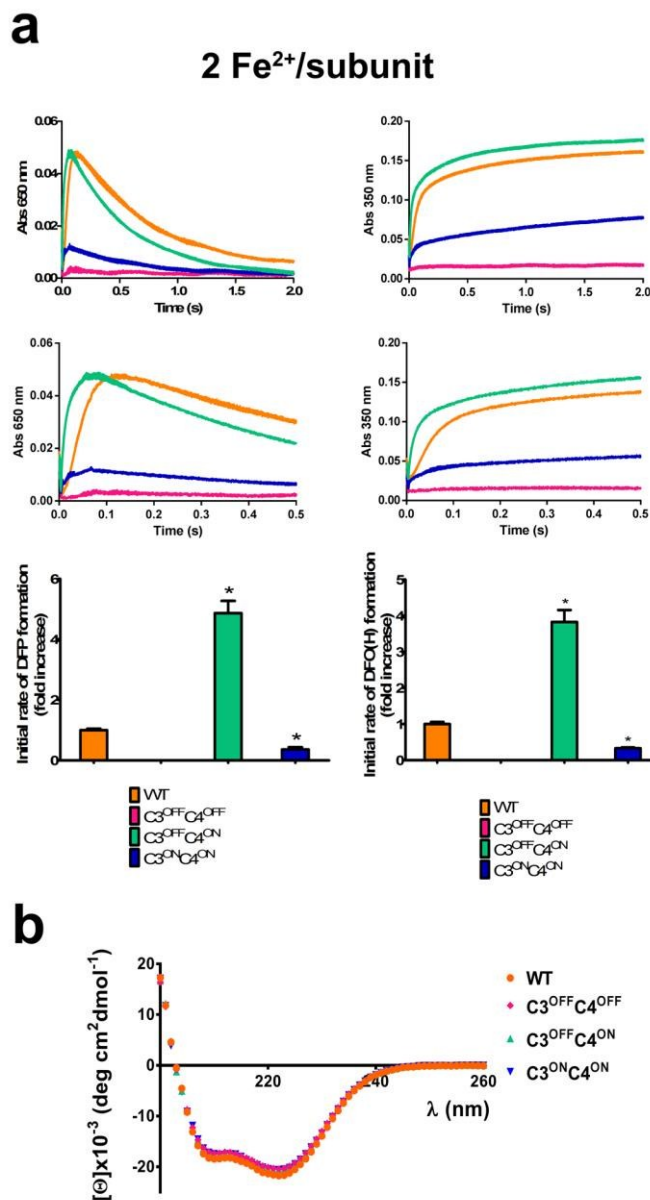


Fig. 3. The pore properties modulate activity in structurally intact ferritin cage variants. (a) Formation of (left) DFP intermediate (A650 nm) and (right) (DFO(H)) products (A350 nm) after the addition of 2 Fe²⁺/subunit. Data are reported for two different time scales: upper panels, 2 s; lower panels, expansion of the initial 0.5 s. Shown are a set of curves (mean ± SEM) of a representative experiment of at least three, each one performed in triplicate, and the corresponding bar plots of the average initial rates. Bars corresponding to the initial rates of the C3^{OFF}C4^{OFF} variant are assumed to be 0 given the absence of any ferroxidase activity of that variant. *Significantly different from the corresponding value in WT (C3^{ON}C4^{OFF}); P < 0.05. (b) The helical content of WT and variant

apoferritins were monitored by CD in the far UV spectral region.

The strong enzymatic activity in C3^{OFF}C4^{ON} cages provided the first experimental proof that the directionality of the iron pathways from the bulk solution to the active site can be efficiently inverted by switching the electrostatic properties of the two classes of channels.

Given the four-fold symmetry of the C4 channels, the M161DL165DH169D (C4^{ON}) variant contains a total of twelve aspartates in the deep end of the channel, which creates a strong attractive electrostatic gradient towards cations. Replacing M161, L165 and H169 (average volume/residue ~ 160-166 Å) with three aspartates (average volume/residue ~ 116 Å)^{20,21}, causes a contextual widening of the C4 channels (Fig. 2) that might also contribute to the significant 5-fold increase in the initial rates of formation of DFP and DFO(H) in C3^{OFF}C4^{ON} ferritin with respect to the WT (C3^{ON}C4^{OFF}) protein (Fig. 3a). X-ray data^{6,9} showed that four symmetry-related H169 residues in C4 channels coordinate iron. This might suggest a role for H169 in iron uptake similar to what observed for E130 and D127 in C3 channels. Nevertheless, as known from previous studies¹⁵ the H169F variant does not alter the ferroxidase activity. Therefore, the Fe²⁺ transit in the C4 channel is not driven by coordination. On the other hand, the present data on the C3^{OFF}C4^{ON} variant show that, channel activation can be achieved by changing the electrostatic properties.

A new cage variant with WT, C3^{ON}, channels and M161DL165DH169D, C4^{ON}, channels was then designed aiming at a super-efficient C3^{ON}C4^{ON} cage (Fig. 2). Surprisingly, in the C3^{ON}C4^{ON} phenotype, the rates of reaction as well as the total amount of formed products with 2 Fe²⁺/subunit drop to values that are only 30% of those in the WT (C3^{ON}C4^{OFF}) cage (Fig. 4a). When the reaction is performed with 4 Fe²⁺/subunit, the reaction efficiency is restored: the initial rate of the C3^{ON}C4^{ON} becomes 1.5 times faster than in WT (C3^{ON}C4^{OFF}); the amount of products formation in the two cages is similar (Fig. 4b).

Mechanistic implications. The mutated residues are all located on helices H4 (D127, E130 and S131) and H5 (M161, L165 and H169). Their substitution with alanine does not affect the 4-helix bundle subunit's structure, as indicated by identical CD spectra in the far UV spectral region (Fig. 3b). The activity of the enzymatic ferroxidase site can be efficiently quenched/restored through barring/debarring the access of ferrous substrates to the cage. In WT (C3^{ON}C4^{OFF}) cages, once ferrous ions have reached the bottom of the C3 channels, they are directed towards the ferroxidase sites under the electrostatic guidance of Glu57 and Glu136 on the cavity wall, just below the dinuclear iron binding sites^{9,22} (Fig. 2c). The ferrous ions then populate the dinuclear centers of the ferroxidase sites (Fig. 1 and Fig. 2c).

The unexpected dependence of the ferroxidase kinetics in the C3^{ON}C4^{ON} cage on the Fe²⁺/subunit ratio is not easy to interpret. In principle, the presence of two types of active channels should produce a cage variant which is more active than any of the others (if the Fe²⁺ fluxes through the two types of channels towards the ferroxidase center can occur

simultaneously) or at least as active as the faster between the C3^{ON}C4^{OFF} and the C3^{OFF}C4^{ON}. In practice, with 2 Fe²⁺/subunit neither of these hypotheses is achieved. However, the C3^{ON}C4^{ON} variant becomes the fastest cage when loaded with 4 Fe²⁺/subunit. The most peculiar feature of C3^{ON}C4^{ON} variant is the increased number of permeable ferrous channels in the cage.

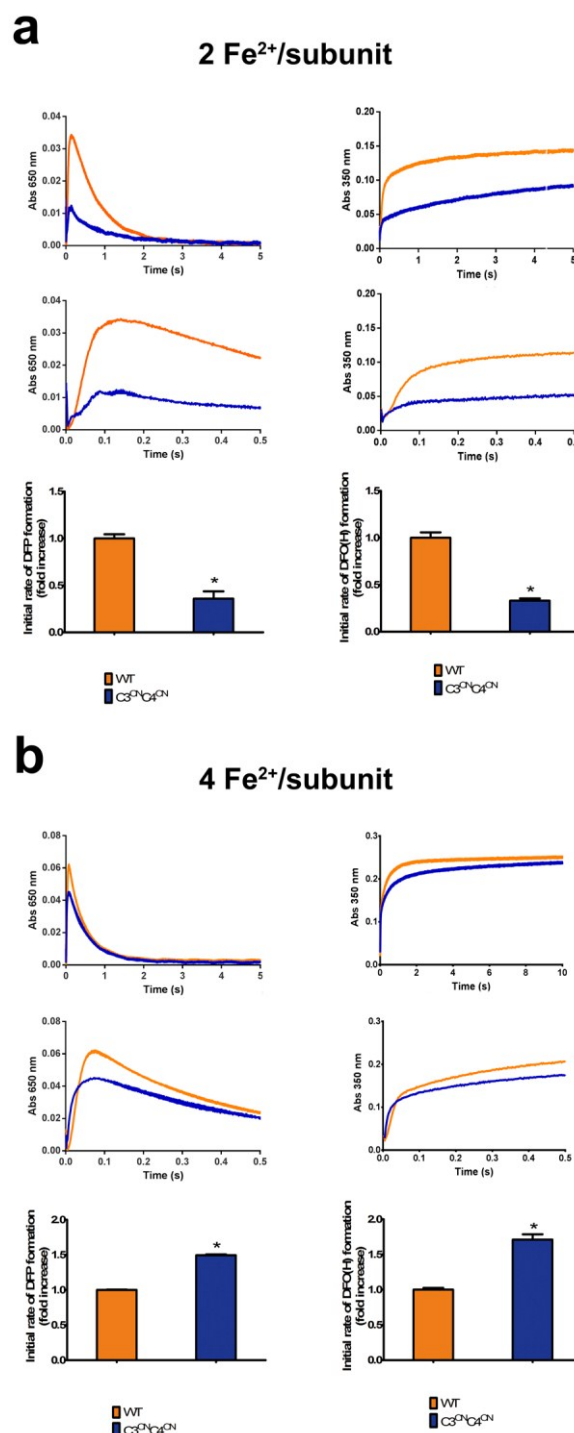


Fig. 4. The ferroxidase reaction rate in WT and C3^{ON}C4^{ON} is differently modulated by the Fe²⁺/subunit ratio. Comparison of the kinetic of (left) DFP intermediate (A_{650 nm}) and (right) (DFO(H)) products (A_{350 nm}) formation between WT (C3^{ON}C4^{OFF}) and C3^{ON}C4^{ON} ferritin variant after the

addition of 2 Fe²⁺/subunit (a) and 4 Fe²⁺/subunit (b). Data are reported for two different time scales: upper panels, 5 s for DFP intermediate and 10 s for DFO(H) products; lower panels, expansion of the initial 0.5 s. Each graph shows a set of curves (mean±SEM) of a representative experiment of at least three, each one performed in triplicate, and corresponding bar plots of the average initial rates. Bar plots report the fold change over WT (set as 1) of the initial rates of formation of the various species, calculated as described in Experimental procedures section from three independent experiments. *Significantly different from the corresponding value in WT (C3^{ON}C4^{OFF}); P < 0.05.

In WT (C3^{ON}C4^{OFF}) and C3^{OFF}C4^{ON} cages, each subunit contributes to the definition of a single negatively charged channel (Fig. 2b and c) and its active site is reasonably receiving ferrous ions from the channel to which the subunit belongs. This strict correspondence is lost in the C3^{ON}C4^{ON} cages, where each subunit contributes to the generation of two different types of negatively charged channels, a C3 one via its H3 and H4 helices and a C4 one via its H5 helix (Fig. 2c); both channels can deliver iron to the same subunit. In the WT (C3^{ON}C4^{OFF}) cages, the ferrous ions that have reached the bottom of the C3 channels move towards the active site under the electrostatic guidance of the negative cluster of residues defined by Glu57/Glu136²² (Fig. 2c), through a well-defined path. An equivalent situation likely occurs for ferrous ions that have reached the bottom of C4 channels in C3^{OFF}C4^{ON} cages and have to travel almost the same distance along the subunit inner surface to reach Glu57/Glu136 and then the active site. Instead, in the C3^{ON}C4^{ON} cages, ferrous ions arrived at the bottom of each type of channel sense two areas of negative electrostatic potentials inside the cavity: the in-pathway Glu57/Glu136 and the off-pathway cluster at the bottom end of the other type of channel. This situation can be detrimental, diverting ferrous ions from their correct track towards the ferroxidase centers.

Additionally, increasing the total number of channels but maintaining the 2 Fe²⁺/subunit ratio reduces the average number of ferrous ions per channel from 6 Fe²⁺/C3 channel in WT (C3^{ON}C4^{OFF}) and 8 Fe²⁺/C4 channel in C3^{OFF}C4^{ON} cages to 3.4 Fe²⁺/C3+C4 channel in the C3^{ON}C4^{ON} cage.

At the present level of knowledge, we cannot exclude the requirement of a minimum number of cations per channel for an efficient rate of delivery to the ferroxidase site. The cooperative binding of the ferrous ions in the active site is demonstrated by the experimental evidence that all Fe1 sites should be first filled before the second ferrous ions binds at Fe2 and reaction occurs^{9,10}. Binding of Fe1 was proposed to increase the affinity of the Fe2 site, leading to concerted binding of Fe2 to form a complete ferroxidase site.⁸ The same authors proposed a Hill coefficient of the order of 3, which should reflect a cooperative interaction among an unidentified subset of subunits⁸. Based on our data, the relevant subset of subunits could be represented by triplets of subunits at the C3 channels; the concerted binding of ferrous substrate into the active site might need metal ions to be imported through the same channel.⁸

With 4 Fe²⁺/subunit, the reaction efficiencies of C3^{ON}C4^{ON} and WT (C3^{ON}C4^{OFF}) become again comparable (Fig. 4b). This could be due to the regaining of a minimum number of Fe²⁺/channels; an average of 6.8 which compares well with the above discussed 6 Fe²⁺/C3 channel in WT (C3^{ON}C4^{OFF}) and 8 Fe²⁺/C4 channel in C3^{OFF}C4^{ON} cages.

Additionally, an increased total number of divalent cations interacting with negative residues at the bottom of the channels can attenuate the off-pathways electrostatic attractions inside the cavity.

Caged biomineral formation. At high iron loading (80 Fe²⁺/subunit), sizeable nanocaged biomineral particles are obtained on a longer time scale (see Experimental procedures) for the ferroxidase-active WT (C3^{ON}C4^{OFF}), C3^{OFF}C4^{ON} and C3^{ON}C4^{ON} cages (Fig. 5a), with average size of 5.52±0.24 nm, 6.05±0.2 nm, and 6.70±0.16 nm, respectively. In the inactive C3^{OFF}C4^{OFF} cage the biomineral is much smaller (3.99±0.26 nm). Stable caged biomineral in non-native cages demonstrates intact assembly and absence of iron spill through the non-WT channels. Particles of a small size, similar to that of C3^{OFF}C4^{OFF} cages, are also observed in the homopolymeric human L ferritin (unpublished results of this lab), which lacks the ferroxidase site. However, using the same biomineralization conditions of the present study for human L ferritin, a heterogeneous distribution of biomineral sizes is observed, ranging from 4 to 7 nm. It should be considered that there are some key differences between a C3^{OFF}C4^{OFF} cage and a cage missing the ferroxidase center as in L ferritin. In the former we slow down the diffusion of iron towards the inner cavity by removing the electrostatic gradient driving force, but we do not inhibit the ferroxidase activity. The latter lacks the ferroxidase center but the channels are intact as well as the cage permeability. It is known that with high Fe²⁺/cage, the slower direct oxidation of ferrous ions on the surface of the biomineral core adds to the fast enzymatic oxidation at the ferroxidase center. The many entry channels in C3^{ON}C4^{ON} cages may facilitate the former mechanism leading to a larger biomineral²³. Nevertheless, by keeping an active ferroxidase center in C3^{OFF}C4^{OFF} cages, mechanistic differences with respect to L ferritin are preserved and the resulting biomineral has different sizes.

Information on the biomineral can also be obtained by magnetic susceptibility measurements in solution, that take advantage of the large paramagnetism of the ferric-oxo nanoparticles. The bulk magnetic susceptibility in solution obtained by Evans measurement results from the average contribution from all the ferritin molecules present in the sample²⁴. The derived effective magnetic moments per subunit (μ_{eff}) increases at increasing iron concentration (Fig. 5b). The inactive C3^{OFF}C4^{OFF} ferritin, where the biomineral growth proceeds via non-enzymatic processes, has a μ_{eff} value significantly lower than the other variants, in agreement with the smaller size of the iron mineral.

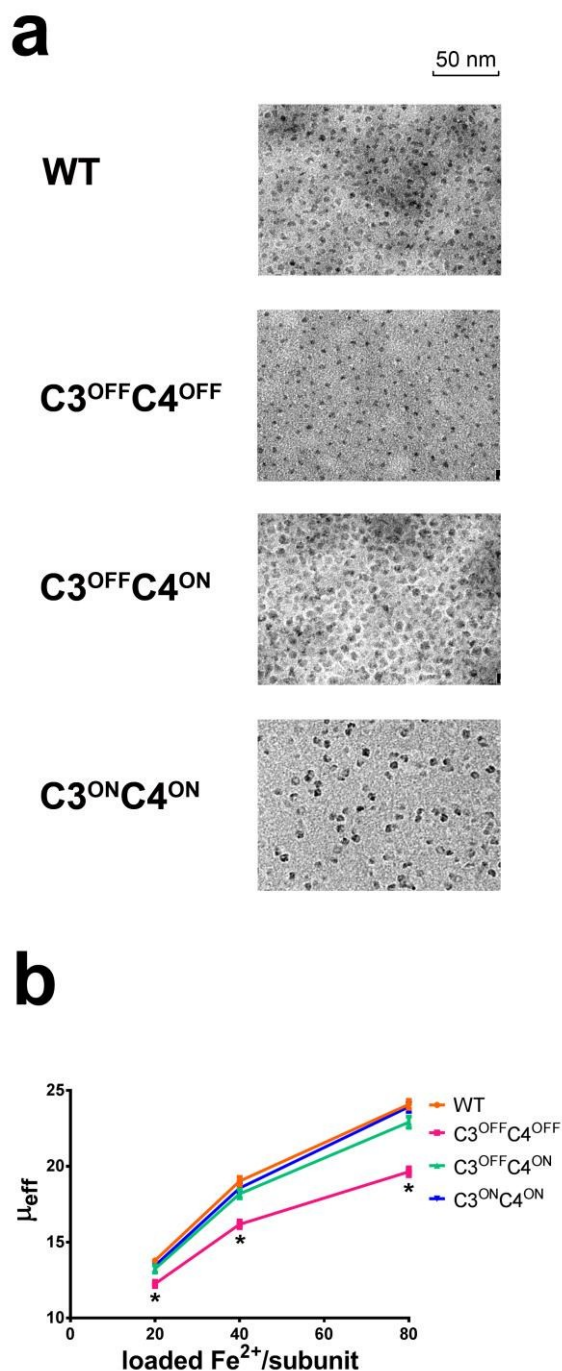


Fig. 5. Biomineral core characterization. (a) Representative TEM micrographs of ferritin caged biomineral obtained from 3 μM solutions of each variant mineralized with ferrous sulfate (80 Fe^{2+} /subunit). The samples are not negatively stained, thus the observed density represents the iron core within ferritin and not the protein. (b) Effective magnetic moments per subunit (μ_{eff}) obtained by Evans measurements at increasing concentrations of iron (20 Fe^{2+} /subunit, 40 Fe^{2+} /subunit and 80 Fe^{2+} /subunit). Data are mean \pm SEM obtained from three independent experiments. *Significantly different from the corresponding value in WT (C3^{ON}C4^{OFF}); $P < 0.05$.

Evolutionary implications. Ferritins have evolved from a common ancestor^{25,26}. According to phylogenetic analyses²⁷,

there are five main divergent branches of the ferritin phylogenetic tree. Here, we have focused on the features of the C3 and C4 channels in representative ferritins of the branches corresponding to bacteria and archaea; to vertebrates; and to green and red algae and land plants (Fig. S1). For all these examples, the 3D structures are available and allow the exact identification of the residues exposed in the interior of the channels. The overall cage architecture is always maintained and the amino acid acting as iron binding ligands in the ferroxidase site of *Rana catesbeiana* H' ferritin are conserved in all the ferroxidase active subunits analyzed. Instead, there are clear differences in the residues inside the channels piercing the protein shell.

The residues in the C3 channel of *Rana catesbeiana* H' ferritin here mutated are largely conserved across the vertebrate ferritins and impart the negative character of the deep end of these channels. An analysis performed on 1000 sequences of vertebrate ferritins (100-26% identity range with respect to the H' ferritin) provided the following results: D127 and E130 are conserved in 73% and 79% of the cases, respectively; the residue in position 131 is a Ser in 21% of the cases and Thr in 45% of the others (another 12% contains an Asn in the corresponding position). For the mutated residues inside the C4, M161 is conserved in 36% of the cases and is a Leu in another 35%; L165 is conserved in 72% of the sequences. H169 is more variable, being present only in 37% of the sequences, in another 20% there is a Leu. In all the here mutated C4 positions the occurrence of Asp or Glu is very uncommon (0.3-0.8%).

In soybean and algal ferritins (Fig. S1), the C3 residues in positions corresponding to D127, E130, S131 are conserved. Conversely, in bacterial ferritins there are no carboxylates at these sites and in the archaea *P. furiosus* there is a single Asp in correspondence to S131; the channel is composed by neutral or even positive residues. This amino acidic composition settles a clear distinction in the nature of the C3 channels between eukaryotic and prokaryotic ferritins, which have likely evolved selecting different types of channel for iron entry.

In vertebrate ferritins the interior of the C4 channels is lined with neutral and, in most cases, hydrophobic residues. The situation is reversed in archaea and bacterial ferritins where the channels are rich in Glu, Ser and Tyr that can exert an electrostatic attraction on the Fe^{2+} ions and allow their transit across the channel. The plant and algal proteins are somehow in between, displaying an increased hydrophilic character of the C4 channels with respect to the vertebrate proteins. Our C3^{OFF}C4^{ON} variant closely resembles the situation of the prokaryotic ferritins, demonstrating that the selection of the C4 as ion accession channels could have been equally possible also for the eukaryotic cage scaffold.

Outlook for the design of ferritin nanocarriers. The ferritin cage represents an interesting carrier for imaging probes, drugs and theranostic agents because the protein shell helps in their efficient solubilization and targeted delivery. Different chemical species can be included in its inner cavity through pH-driven disassembly and reassembly processes followed by purification procedures, whereas free diffusion through the

cage is limited to relatively small and cationic ions that can enter the cage through the C3 ion channels²⁸. Here, we demonstrated the possibility to maintain an intact structure in the presence of fully neutral and essentially hydrophobic C3 and C4 channels (in the C3^{OFF}C4^{OFF} ferritin variant), sensibly wider C3 channels (in all the C3^{OFF} ferritin variants) and wider negatively charged C4 channels (in all the C4^{ON} ferritin variants) (see legend to Fig. 2 for the average channel sizes in the WT cage and its variants). Modulation of channel hydrophilicity is expected to be important for the development of high-sensitivity magnetic resonance imaging probes based on paramagnetic metal ions because able to influence the exchange between bulk water and water confined inside the cage²⁹. T₁ relaxivity data were acquired on the present cage variants reacted with 20 Fe²⁺/subunit over the magnetic field range 0–100 MHz. At 35 °C and in the magnetic field range relevant for MRI (i.e., 1–3 T) the paramagnetic contribution to T₁⁻¹, normalized with respect to the effective magnetic moment (Fig. 5), decreases in the order WT ~ C3^{ON}C4^{ON} > C3^{OFF}C4^{ON} > C3^{OFF}C4^{OFF}. The latter variant contains the most hydrophobic channels. Therefore, taking the C3^{OFF}C4^{OFF} ferritin variant relaxivity as reference level, we observed that the contribution of the 8 negatively-charged C3^{ON} channels in the WT (C3^{ON}C4^{OFF}) ferritin accounts for a 3-fold increase in relaxivity, whereas the activation of the 6 negatively-charged C4^{ON} channels in the C3^{OFF}C4^{ON} ferritin variant accounts for a 2-fold increase. Other factors beyond the charges in the channels and the channel size seem therefore important in modulating inner/outer water exchange. This aspect could be further exploited in future studies aimed at the development of new MRI probes. Synthesis of inorganic cores directly inside the ferritin cage has been also exploited with the aim to produce nanoscale soluble minerals using metal ions that are not substrates for the ferroxidase site. The electrostatic potential on the inner surface of ferritin is important to attract metal ions and to initiate the nucleation of the inorganic material²⁸. The ferritin variants here characterized contain differently charged residues in the deep ends of C3 and C4 channels that may contribute in both aspects of the mechanism of the inorganic core formation.

Conclusions

The presence of carboxylates at the inner edge of the C3 and C4 channels determines an electric field gradient between the outer and inner channel sides that is responsible of the “gated” entry of Fe²⁺ ions into the cage. Negative charges in place of neutral residues inside the C4 channels establish new iron pathways that allow ferrous ions to cross the protein shell down their electrochemical gradients and then to proceed towards the ferroxidase sites. The rate of the flux of ions through the channels influences the rate of the catalytic oxidation; the best efficiency of the ferroxidase reaction is achieved avoiding competing ferrous routes.

Prokaryotic, plant, and animal ferritins differ in the ion channel (Fig. S1): in prokaryotes the negative iron channels are at C4³⁰.

³¹; both C3 and C4 channels allow iron transit in photosynthetic eukaryotes³². Vertebrate ferritin evolution has led to the selection of C3 as the Fe²⁺ entry channels^{6,9-15,17-19}, but we have here demonstrated that both the other alternative solutions would have been equally possible.

From an applicative point of view, the ability to modulate the channels’ properties (size and electrostatics) is important for the design of novel ferritin-based nanocarriers able to efficiently import and retain cargo molecules of different size and charge^{33,34}.

Experimental procedures

Mutagenesis. Site directed amino acid substitutions in *Rana catesbeiana*-H’ ferritin protein cages were generated by PCR, using the QuikChange II site-directed mutagenesis kit (Stratagene). The DNA in the coding regions in all the protein expression vectors was analyzed for sequence confirmation (Primm srl, Milan, Italy).

Protein Expression. pET-3a constructs encoding WT and variant *Rana catesbeiana*-H’ ferritins were transformed into *Escherichia coli* BL21(DE3) pLysS cells which were subsequently cultured in LB medium containing ampicillin (0.1 mg ml⁻¹) and chloramphenicol (34 µg ml⁻¹). Cells were grown at 37 °C, until A_{600nm} reached 0.6–0.8 and subsequently induced with isopropyl 1-thio-β-D-galactopyranoside (IPTG, 1 mM final concentration) for 4 h. Recombinant ferritins were purified from the harvested cells, as described previously^{24,35}.

Circular Dichroism Spectroscopy. CD spectra were acquired in the far-UV with a Jasco J-810 spectropolarimeter using a 0.1 cm path length quartz cuvette and 20 µM protein concentration (in subunits) in 20 mM Tris buffer, pH 7.5 at 25 °C⁵. The mean of 10 scans between 200 and 260 nm wavelength was calculated by subtraction of the corresponding buffer spectrum.

Stopped-flow kinetics. Single¹⁵- or double³⁶-turnover catalysis (2 Fe²⁺ ions per subunit or 4 Fe²⁺ ions per subunit), in *Rana catesbeiana* H’ ferritin, WT or with amino acid substitutions, was monitored as the change in A_{650 nm} (DFP) or A_{350 nm} (DFO(H)) after rapid mixing (less than 10 ms) of equal volumes of 100 µM protein subunits (4.16 µM protein cages) in 200 mM 3-(N-morpholino)propanesulfonic acid (MOPS), 200 mM NaCl, pH 7.0, with freshly prepared solutions of 200 µM ferrous sulfate or 400 µM ferrous sulfate in 1 mM HCl in a UV-visible stopped-flow spectrophotometer (SX.18MV stopped-flow reaction analyzer, Applied Photophysics, Leatherhead, UK). Routinely, 4000 data points were collected during the first 2 s. Initial rates of DFP and DFO(H) species formation were determined from the linear fitting of the initial phases of the 650- and 350-nm traces (0.01–0.03 s).

Transmission Electron Microscopy. Recombinant ferritin protein cages (3 µM) were mineralized with ferrous sulfate (80 Fe²⁺/subunit) in 100 mM MOPS, 100 mM NaCl, pH 7.0⁵. After mixing, the solutions were incubated for 2 h at room temperature and then overnight at 4 °C to complete the iron mineralization reaction. Solutions of mineralized WT and variant ferritin cages were dropped and dried on a Cu grid

covered by holey carbon film. Bright-field TEM images were collected on a Philips CM12 microscope operating at 80 kV_a.

Magnetic Susceptibility Measurements. The magnetic susceptibility of ferritin with increasing amounts of iron was measured by the modified Evans method³⁷ as previously reported^{24,38}. Coaxial NMR tubes were used with 1,4-dioxane as internal reference. The paramagnetic and diamagnetic protein samples were prepared from the same stock solution of apoprotein. Samples were 288 μM in subunit monomer in 100 mM of MOPS, pH 7 and 5 mM of 1,4-dioxane. The apoprotein solution (obtained through exhaustive dialysis) was split into two aliquots: the diamagnetic apoferritin solution in the inner capillary; in the outer tube mineralized ferritin with increasing Fe²⁺/subunit, mineralized as described above. The ¹H chemical shift of 1,4-dioxane was measured on the 16.4-T Bruker AVANCE 700 spectrometer at 300 K. The entire set of Evans measurements was repeated three times. The inner-outer tube peak separation ($\Delta\delta$, expressed in ppm) was measured, assigned to the bulk susceptibility shift, and used to calculate μ_{eff} ²⁴.

Structure modeling of the ferritin variants. To help visualizing the effect on the surface electrostatic potentials induced by our mutations, structure modeling of the ferritin variants (C3^{OFF}C4^{OFF}, C3^{ON}C4^{OFF}, C3^{ON}C4^{ON}) was performed with Modeller v9.11³⁹, using the molecular dynamics (MD) annealing protocol. The best structure for each variant was chosen among 50 models as the one with the lowest DOPE (Discrete Optimized Protein Energy) potential. To avoid steric clashes, selected models were then subjected to energy minimization using AMBER 14 (ff99sb force field and explicit water), through the AMPS-NMR web portal⁴⁰.

Sequence alignment. The analysis of conservation of the mutated residues was performed searching for ferritins from vertebrate sequences in UniProtKB database by BLAST; multiple sequence alignment was obtained by ClustalW⁵. The data reported are the result obtained using the 1000 sequences that have identity range 100–26% to the H' ferritin here studied.

Statistical analysis. The data were analyzed by Student's *t* test, and *P* < 0.05 was considered significant.

Relaxivity measurements. Longitudinal water proton relaxation rates (T_1^{-1}) profiles were measured with a prototype of a Stellar fast field cycling relaxometer over the 0.01–40 MHz proton Larmor frequency range⁴¹. The instrument provides T_1^{-1} values with an error smaller than 1%. Relaxivity data were acquired on solutions 6 μM of the WT and variant ferritins loaded with 20 Fe²⁺/subunit. The paramagnetic contribution to the total relaxivity was derived by subtracting from the measured T_1^{-1} the corresponding values obtained for equimolar solutions of the diamagnetic apoferritins.

Acknowledgements

We acknowledge the financial support of MIUR PRIN 2012 (contract number 2012SK7ASN). C.B. is the recipient of a post-doctoral fellowship funded by Ente Cassa di Risparmio di Firenze (contract number 2013.0494).

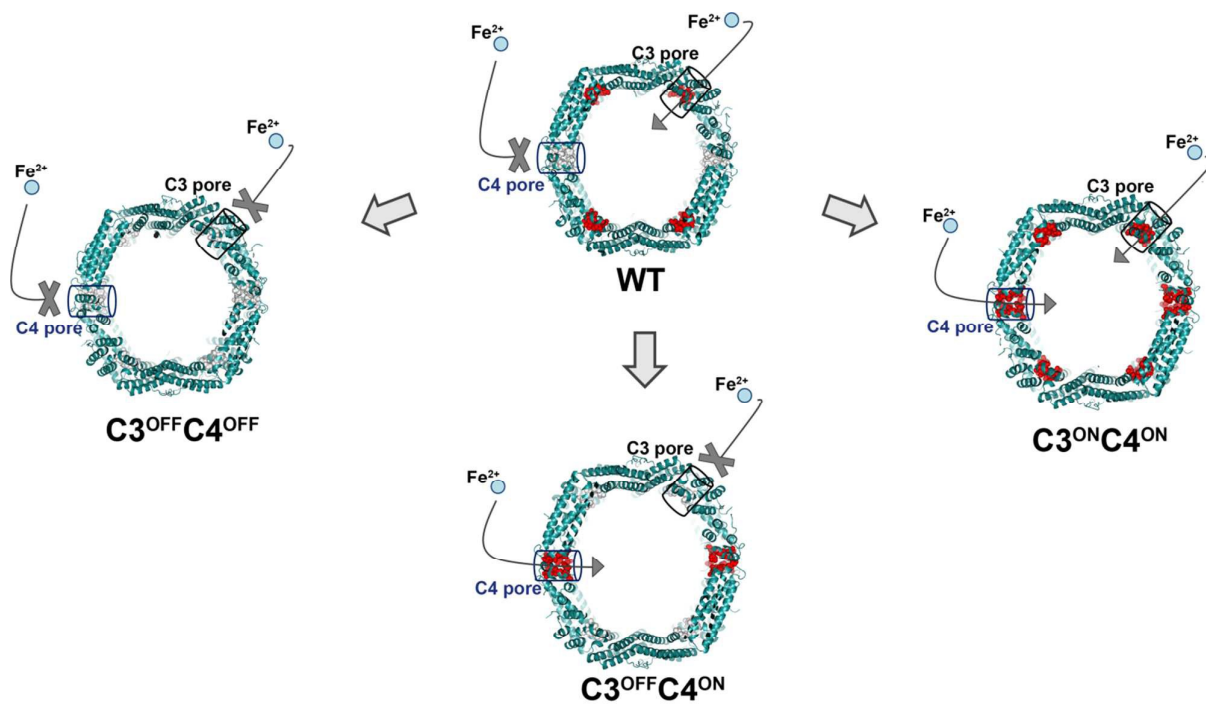
References

- D.J. Huard, K.M. Kane and F.A. Tezcan, *Nat Chem Biol*, 2013, **9**, 169.
- E.C. Theil, R.K. Behera and T. Tosha, *Coord Chem Rev*, 2013, **257**, 579.
- R.R. Crichton and J.P. Declercq, *Biochim Biophys Acta*, 2010, **1800**, 706.
- D. Lalli and P. Turano, *Acc Chem Res*, 2013, **46**, 2676.
- C. Bernacchioni, V. Ghini, C. Pozzi, F. Di Pisa, E.C. Theil and P. Turano, *ACS Chem Biol*, 2014, **9**, 2517.
- I. Bertini, D. Lalli, S. Mangani, C. Pozzi, C. Rosa, E.C. Theil and P. Turano *J Am Chem Soc*, 2012, **134**, 6169.
- J. Hwang, C. Krebs, B.H. Huynh, D.E. Edmondson, E.C. Theil and J.E. Penner-Hahn, *Science*, 2000, **287**, 122.
- J.K. Schwartz, X.S. Liu, T. Tosha, E.C. Theil and E.I. Solomon, *J Am Chem Soc*, 2008, **130**, 9441.
- C. Pozzi, F. Di Pisa, D. Lalli, C. Rosa, E.C. Theil, P. Turano and S. Mangani *Acta Crystallogr. D*, 2015, **71**, 941.
- C. Pozzi, F. Di Pisa, C. Bernacchioni, S. Ciambellotti, P. Turano and S. Mangani, *Acta Crystallogr. D*, 2015, **71**, 1909.
- X. Liu and E.C. Theil, *Acc Chem Res*, 2005, **38**, 167.
- E.C. Theil, *Curr Opin Chem Biol*, 2011, **15**, 304.
- S. Haldar, L.E. Bevers, T. Tosha and E.C. Theil, *J Biol Chem*, 2011, **286**, 25620.
- T. Tosha, R.K. Behera and E.C. Theil, *Inorg Chem*, 2012, **51**, 11406.
- E.C. Theil, P. Turano, V. Ghini, M. Allegrozzi and C. Bernacchioni, *J Biol Inorg Chem*, 2014, **19**, 615.
- T. Takahashi and S. Kuyucak, *Biophys J*, 2003, **84**, 2256.
- S. Levi, P. Santambrogio, B. Corsi, A. Cozzi and P. Arosio, *Biochem J*, 1996, **15**, 467.
- F. Bou-Abdallah, P. Arosio, S. Levi, C. Janus-Chandler, N.D. Chasteen, *J Biol Inorg. Chem*, 2003, **8**, 489.
- F. Bou-Abdallah, G. Zhao, G. Biasiotto, M. Poli, P. Arosio and N.D. Chasteen, *J Am Chem Soc*, 2008, **130**, 17801.
- A.E. Counterman and D.E. Clemmer, *J. Am. Chem. Soc.*, 1999, **121**, 4031.
- J. Tsai, R. Taylor, C. Chothia and M. Gerstein, *J Mol Biol*, 1990, **290**, 253.
- R.K. Behera and E.C. Theil, *Proc Natl Acad Sci U S A*, 2014, **111**, 7925.
- R.K. Watt, R.J. Hilton and D.M. Graff, *Biochim Biophys Acta*, 2010, **1800**, 745.
- P. Turano, D. Lalli, I.C. Felli, E.C. Theil and I. Bertini, *Proc Natl Acad Sci U S A*, 2010, **107**, 545.
- S.C. Andrews, *Biochim Biophys Acta*, 2010, **1800**, 691.
- D. Lundin, A.M. Poole, B.M. Sjöberg and M. Högbom, *J Biol Chem*, 2012, **287**, 20565.
- A. Marchetti, M.S. Parker, L.P. Moccia, E.O. Lin, A.L. Arrieta, F. Ribalet, M.E. Murphy, M.T. Maldonado and E.V. Armbrust, *Nature*, 2009, **457**, 467.
- G. Jutz, P. van Rijn, B. Santos Miranda and A. Böker, *Chem Rev*, 2015, **115**, 1653.
- O. Vasalatiy, P. Zhao, S. Zhang, S. Aime and A.D. Sherry, *Contrast Media Mol Imaging*, 2006, **1**, 10.
- K.J. Cho, H.J. Shin, J.H. Lee, K.J. Kim, S.S. Park, Y. Lee, C. Lee, S.S. Park and K.H. Kim, *J Mol Biol*, 2009, **390**, 83.
- F. Bou-Abdallah, *Biochim Biophys Acta*, 2010, **1800**, 719.
- C. Lv, S. Zhang, J. Zang, G. Zhao and C. Xu, *Biochemistry*, 2014, **53**, 2232.
- J.O. Jeon, S. Kim, E. Choi, K. Shin, K. Cha, I.S. So, S.J. Kim, E. Jun, D. Kim, H.J. Ahn, B.H. Lee, S.H. Lee and I.S. Kim, *ACS Nano*, 2013, **7**, 7462.
- S. Aime, L. Frullano and S. Geninatti Crich, *Angew Chem Int Ed Engl*, 2012, **41**, 1017.
- M. Matzapetakis, P. Turano, E.C. Theil and I. Bertini, *J Biomol NMR*, 2007, **38**, 237.

ARTICLE

RSC Advances

- 36 C. Bernacchioni, S. Ciambellotti, E.C. Theil and P. Turano *Biochim Biophys Acta*, 2015, **1854**, 1118.
- 37 D.F. Evans, *J Chem Soc*, 1959, 2003.
- 38 I. Bertini, C. Luchinat, P. Turano, G. Battaini, and L. Casella, *Chemistry*, 2003, **9**, 231.
- 39 A. Sali, L. Potterton, F. Yuan, H. van Vlijmen and M. Karplus, *Proteins*, 1995, **23**, 318.
- 40 I. Bertini, D.A. Case, L. Ferella, A. Giachetti and A. Rosato, *Bioinformatics*, 2011, **27**, 2384.
- 41 I. Bertini, C. Luchinat and G. Parigi, *Solution NMR of Paramagnetic Molecules*, Elsevier, Amsterdam, 2001.



Electric field gradients across the C3 and C4 ferritin channels controls the directional Fe^{2+} fluxes towards the catalytic ferroxidase center.